Journal of Power Sources 246 (2014) 192–197

Contents lists available at ScienceDirect

Journal of Power Sources

journal homepage: www.elsevier.com/locate/jpowsour

Short communication

Solid-state synthesis of uniform Li_2MnSiO_4/C/graphene composites and their performance in lithium-ion batteries

Huaxu Gong [a], Yongchun Zhu [a,*], Linlin Wang [a], Denghu Wei [a], Jianwen Liang [a], Yitai Qian [a,b]

[a] Hefei National Laboratory for Physical Science at Microscale, Department of Chemistry, University of Science and Technology of China, Hefei, Anhui 230026, PR China
[b] School of Chemistry and Chemical Engineering, Shandong University, Jinan 250100, PR China

HIGHLIGHTS

- Li_2MnSiO_4/C nanospheres have uniform spherical morphology and size of 50 nm.
- The nanospheres are embedded in the 3D nest-like carbon network.
- Li_2MnSiO_4/C/graphene composites have good electrochemical performance.
- Carbon network and carbon coating are favorable for improving the cyclability.

GRAPHICAL ABSTRACT

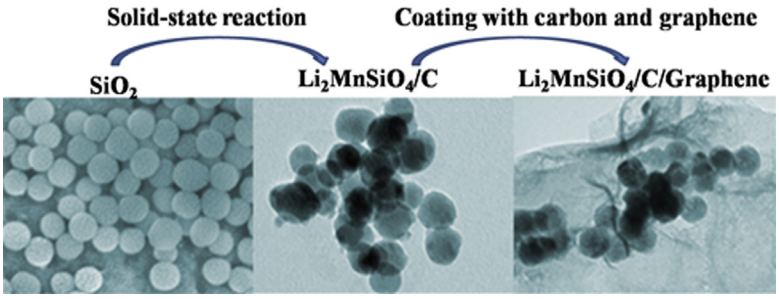

ARTICLE INFO

Article history:
Received 20 April 2013
Received in revised form
31 May 2013
Accepted 22 July 2013
Available online 31 July 2013

Keywords:
Composites
Nanospheres
Carbon network
Electrochemical properties

ABSTRACT

Uniform nanospherical Li_2MnSiO_4/C/graphene composites have been obtained by polyethylene glycol-600 (PEG-600) assisted solid-state reaction using spherical SiO_2 as precursor, and heat treatment with the mixed carbon sources (glucose, cellulose acetate and graphene oxide). The transmission electron microscope (TEM) images show that Li_2MnSiO_4 nanospheres with size of 50 nm are embedded in the three-dimensional (3D) nest-like carbon network. Electrochemical measurements reveal that the composites exhibit first discharge capacity of 215.3 mAh g^{-1} under 0.05 C, together with a stable discharge capacity of 175 mAh g^{-1} after 40 cycles. The 3D carbon network and the carbon layer (amorphous carbon and graphene) are favorable for improving the electrochemical performance.

1. Introduction

As a class of cathode materials for lithium-ion batteries (LIBs), Li_2MSiO_4 (M = Mn, Fe, Co, Ni) [1–4] family have attracted wide attention, and Li_2MnSiO_4 is a good choice among Li_2MSiO_4 family due to its high cell voltage (Mn^{2+}/Mn^{3+} and Mn^{3+}/Mn^{4+}) [5], and high theoretical capacity of 333 mAh g^{-1} (extracting more than one Li^+ ion per formula unit). However, the poor conductivity (low electronic conductivity, slow diffusion of lithium ions) [6] has prevented its further use in commercial applications.

Usually, the decrease in particle size coupled with coating carbon is an effective way to overcome those drawbacks and improve the electrochemical performance [7,8]. Various synthesis methods have been applied to synthesize Li_2MnSiO_4, such as solvothermal route [9,10], sol–gel method [11], solid-state reaction [12] and so on. Among those synthesis methods, solid state route is a

* Corresponding author. Tel.: +86 0551 360 1589; fax: +86 551 360 0006.
E-mail address: ychzhu@ustc.edu.cn (Y. Zhu).

0378-7753/$ – see front matter © 2013 Elsevier B.V. All rights reserved.
http://dx.doi.org/10.1016/j.jpowsour.2013.07.079

conventional synthesis method and appropriate technique for production in large scale. For instance, irregular and aggregated Li_2MnSiO_4 particles with size of 0.1 um–5 um were obtained by solid-state reaction [13], which exhibited a first discharge capacity of 153 mAh g^{-1} under a current density of 10 mA g^{-1}. Carbon coated Li_2MnSiO_4 with uneven size around 20 um synthesized through solid-state method showed a discharge capacity of 140 mAh g^{-1} at 1/20 C [14]. As mentioned above we find that the products obtained by the solid-state reaction under high temperature are usually irregular and aggregated particles, very few reports could be traced for the controlling particle morphology and the size less than 100 nm under solid-state approaches.

Carbon coating is known as one of the simplest and most effective way to improve the cycling stability and rate capability of Li_2MnSiO_4. For example, carbon-coated Li_2MnSiO_4 powder was prepared using adipic acid as carbon source [15], which exhibited a discharge capacity of 181 mAh g^{-1} at the first cycle, and 150 mAh g^{-1} on the 13th cycle under a current density of 1 mA cm^{-2}. The mixed carbon source is also used to improve the cycling stability of Li_2MnSiO_4. For example, a lot of ketjen black and Teflonized acetylene black were used together to improve the cycling stability of Li_2MnSiO_4 [16], and the as prepared Li_2MnSiO_4/C (42% carbon) composite exhibited a stable discharge capacity of about 140 mAh g^{-1} for 40 cycles at 0.05 C. Recently, graphene has shown great potential in LIBs applications due to the high conductivity of graphene sheets, and the electrochemical performance of some electrode materials (such as $LiFePO_4$ [17,18], Fe_3O_4 [19], Co_3O_4 [20]) has been improved after combined with graphene.

Herein, we synthesized uniform nanospherical Li_2MnSiO_4/C/graphene with size of 50 nm. Firstly, uniform nanospheres of Li_2MnSiO_4/C with size of 50 nm were obtained by a modified solid-state method in the presence of PEG-600, and the TEM images showed that Li_2MnSiO_4 nanospheres are loaded and dispersed within the 3D nest-like carbon network. Then, Li_2MnSiO_4/C/graphene composites were obtained through anneal treatment with mixed carbon sources (glucose, cellulose acetate and graphene oxide). As cathode materials for LIBs, the composites delivered first discharge capacity of 215.3 mAh g^{-1} under 0.05 C, together with a stable reversible capacity of 175 mAh g^{-1} after 40 cycles. It was found that the morphology of the composites after 10 cycles was basically maintained, suggesting that this structure is effective in preventing the aggregation of Li_2MnSiO_4 particles during the charge/discharge process.

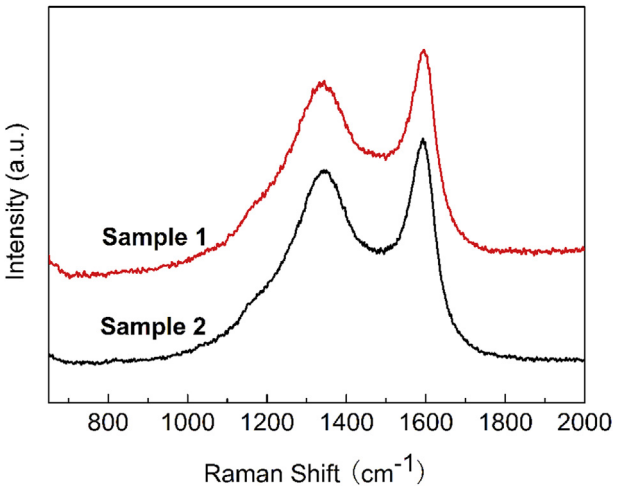

Fig. 2. Raman spectra of the sample 1 and sample 2.

2. Experimental

2.1. Synthesis precursor of SiO_2 nanospheres

The SiO_2 nanospheres were synthesized by the well known Stöber method [21]. 158 mL absolute ethanol, 7.8 mL ammonia, and 2.8 mL distilled water were introduced in a 250 mL round-bottom flask and heated to 50 °C under stirring, then 5.8 mL tetraethyl orthosilicate (TEOS) was added into the solution and stirred at 50 °C for 24 h; SiO_2 spheres were obtained by drying the white solution at 70 °C for 24 h.

2.2. Synthesis of Li_2MnSiO_4/C nanospheres

Stoichiometric amount of SiO_2 (as-prepared), $MnCO_3$, $LiOH \cdot H_2O$ and 0.5 mL Polyethylene Glycol-600 (PEG-600) were mixed

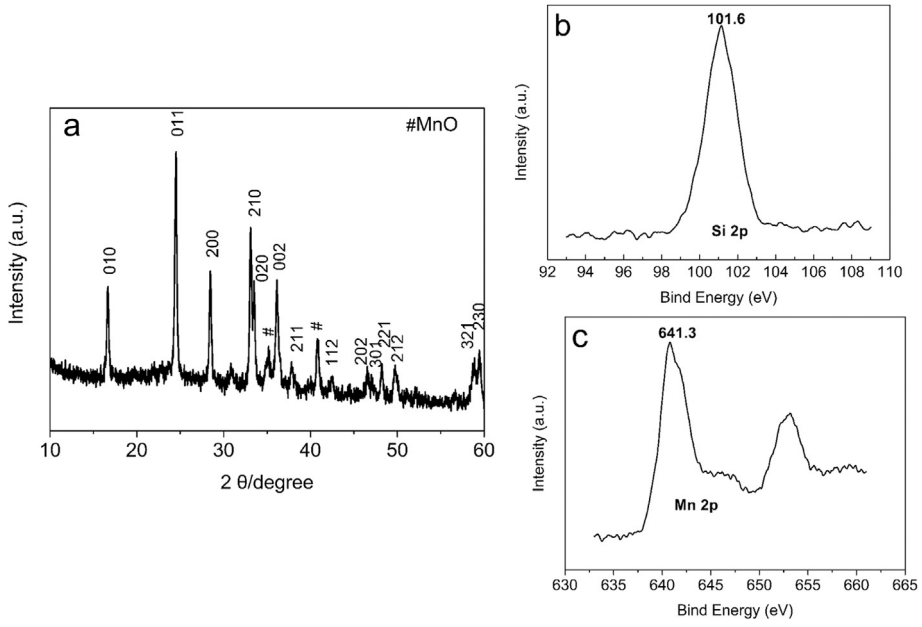

Fig. 1. (a) XRD pattern of the sample 1, (b, c) XPS spectra of sample 1.

together and treated by ultrasonic for 0.5 h, and the mixture was heated at 260 °C 0.5 h, 270 °C 1 h and 400 °C 2 h under Ar/H_2 (5 wt %, H_2) atmosphere. Then the intermediate product was ground and calcined at 700 °C for 8 h in Ar/H_2 (5 wt%, H_2) atmosphere to obtain Li_2MnSiO_4/C nanospheres (denoted by sample 1).

2.3. Synthesis of Li_2MnSiO_4/C/graphene nanospheres

Preparation of graphene oxide (GO): Graphene oxide (GO) was prepared following the procedure described in previous report [22]. The as-prepared graphene oxide powder was added into distilled water and treated by ultrasonic. The final suspension of GO was concentrated to a content of 6 wt%.

Aqueous suspension of GO, sample 1, glucose and cellulose acetate (sample 1: glucose:cellulose acetate:GO = 10:1:1: 0.5 (wt.)) were stirred together to form a slurry. Thereafter, the slurry was ultrasonically exposed for 20 min, and then dried at room temperature to form solid composites. The composites were annealed at 400 °C for 4 h in Ar atmosphere to get Li_2MnSiO_4/C/graphene composites finally (denoted by sample 2).

2.4. Materials characterization

X-ray powder diffraction (XRD) patterns of the products were recorded on a Philips X'pert X-ray diffractometer with Cu Kα radiation (λ = 1.54182 Å). X-ray Photoelectronic Spectrum measurements (XPS) were performed by using a VGESCA-LABMKIIX-ray photoelectronic spectrometer, using non-monochromated Mg Kα X-ray radiation as the excitation source. Raman spectrums were carried out on a JY LABRAM-HR confocal laser micro-Raman spectrometer using Ar^+ laser excitation with a wavelength of 514.5 nm. The microstructure was observed with a field-emitting scanning electron microscope (SEM, JEOL-JSM-6700F), a transmission electron microscope (TEM, H7650), and a high-resolution transmission electron microscope (HRTEM, JEOL-2010) with an accelerating voltage of 200 kV. Elemental analyses were carried out on a vario EL-III elemental analyzer (Germany).

Charge/discharge tests were carried out using CR 2016 coin-type cells. The active material, acetylene black and polyvinylidene fluoride (PVDF) with a weight ratio of 68:22:10 were mixed homogeneously with *N*-methyl-pyrrolidone, and the obtained slurry

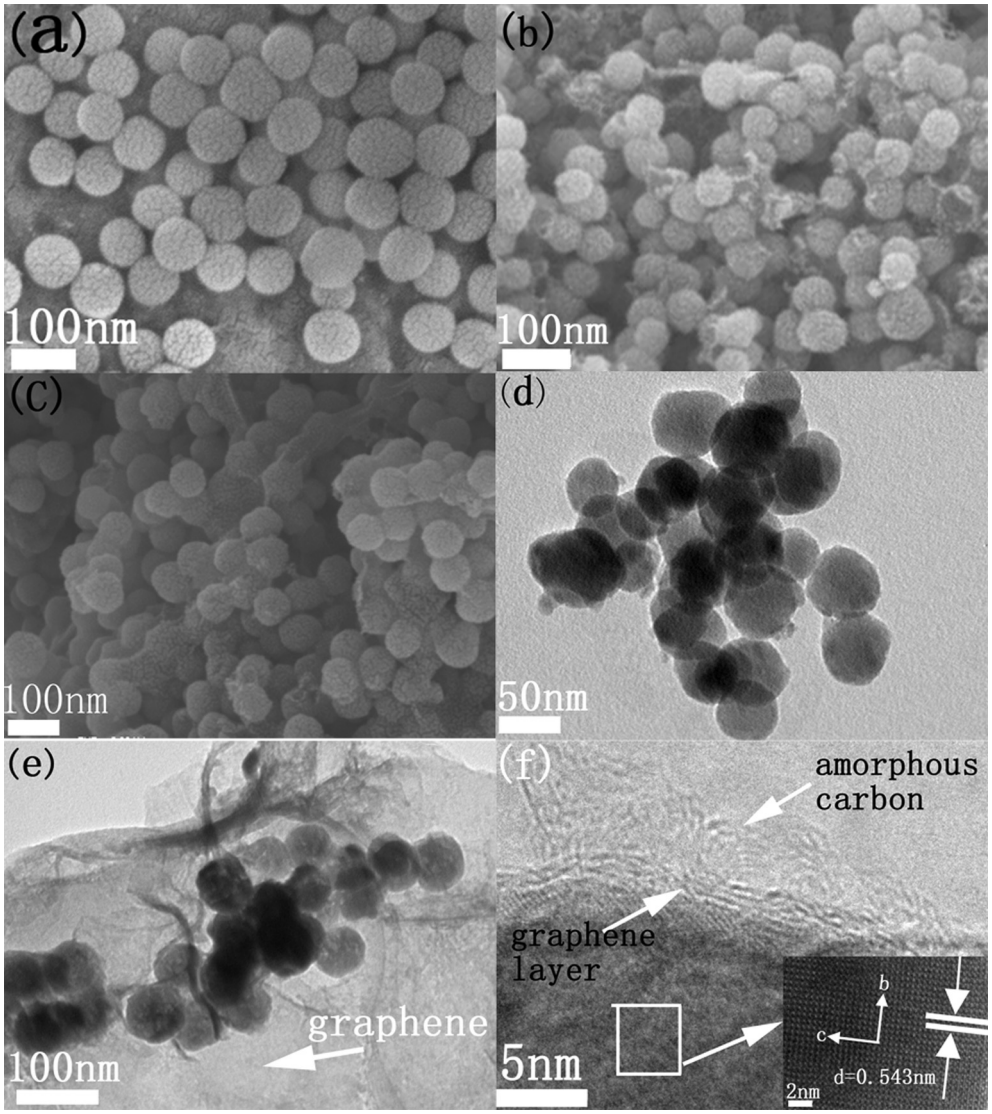

Fig. 3. (a, b and c) Scanning electron microscopy (SEM) images of SiO_2, sample 1 and sample 2; (d, e) Transmission electron microscope (TEM) images of sample 1 and sample 2, (f) HRTEM image of sample 2.

was pasted on Al foil and dried at 110 °C for 12 h in vacuum. The electrode sheet typically had an active material of 1–2 mg cm^{-2}. The coin cell was assembled in an argon-filled glove box (Mikrouna, Super 1220/750/900, China) and consist of Li_2MnSiO_4 (cathode), Celgard 2400 (separator), and lithium foil (anode). 1 mol L^{-1} solution of $LiPF_6$ dissolved in ethylene carbonate/dimethyl carbonate (EC/DMC) (1:1 volume ratio) was used as the electrolyte. Galvanostatic charge/discharge measurements were performed in a potential range of 2–4.6 V at room temperature on a LAND-CT2001A instrument, and the final capacities were calculated based on weight of the Li_2MnSiO_4. The impedance spectroscopy (EIS) was recorded with an electrochemical workstation (Chenhua, Shanghai).

3. Results and discussion

Fig. 1a shows the XRD pattern of sample 1. The crystalline peaks can be identified as orthorhombic Li_2MnSiO_4 with a space group of $Pmn2_1$, which is analogous to the β-Li_3PO_4 pattern [23]. The calculated cell parameters are: a = 6.324 Å, b = 5.330 Å and c = 4.953 Å, these results are in good agreement with values published by previous literature [12,24]. Additional peak marked by "#" in the pattern can be identified as MnO. Similar impurity phases are also appeared in other reports [14–16,23,25,26]. The XPS spectra of sample 1 are shown in Fig. 1b, c. The binding energy of Mn $2p_{3/2}$ (641.3 eV) is corresponding to Mn^{2+}, showing that the divalent state of manganese in our samples. The binding energy of Si 2p (101.6 eV) is in line with that of Si^{4+} in polysiloxane, indicating the formation of the orthosilicate structure [SiO_4] [12].

Fig. 2 is the Raman spectra of sample 1 and sample 2, they have similar Raman spectra. Two obvious peaks at 1358 and 1590 cm^{-1} corresponding to D-band and G-band, respectively [27], revealing the presence of carbon in the samples. The D-band comes from disorder in the sp^2-hybridized carbon, while the G-band is related to the tangential stretching (E_{2g}) mode of graphite. The I_D/I_G ratio of the sample 1 and sample 2 are 1.70 and 1.78, indicating that as-obtained samples possess disorder and defects carbon. The carbon contents of sample 1 and sample 2 are confirmed to be 13.7 wt % and 16.2 wt% respectively by elementary analysis.

Fig. 3 shows the SEM and TEM images of SiO_2 precursor and as obtained products. The monodisperse SiO_2 precursor exhibits spherical morphology with an average diameter of 50 nm (Fig. 3a). After the solid-state reaction, the particles of sample 1 have similar morphology and size to those of SiO_2 precursor (Fig. 3b). The TEM image of sample 1 (Fig. 3d) further confirms that the particles exhibit uniform morphology and size of 50 nm. After coating with carbon and graphene (Fig. 3c, e), the morphology and size of sample 2 basically keep unchanged and present uniform morphology (Fig. 3c). The TEM image (Fig. 3e) and HRTEM image (Fig. 3f) of sample 2 clearly reveal the presence of carbon and graphene sheets. In Fig. 3e, we can find out that spherical nanoparticles are coated with carbon and graphene sheets. As seen from the HRTEM image in Fig. 3f, we further confirm that the sample 2 is enwrapped by a thin carbon layer. The carbon layer consists of 3 layers of graphene and an amorphous carbon layer with a thickness of about 3 nm (which is resulted from the decomposition of glucose and cellulose acetate). The interlayer distance is measured to be about 0.371 nm, which is close to the graphite lattice spacing of d_{0002} (0.340 nm). The inset of Fig. 3f displays regular interface distance of 0.536 nm, which is corresponding to the (010) plane of orthorhombic Li_2MnSiO_4.

The spherical morphology and the size distribution of Li_2MnSiO_4 nanoparticles were found to be strongly dependent on the presence of PEG-600. In absence of PEG-600, the Li_2MnSiO_4 was also obtained but the products were irregular and agglomerated particles (Fig. 4a). It was known that the PEG-600 would act as a complexing agent to promote the formation of a homogeneous phase during reaction [28]. In the beginning of the reaction, with

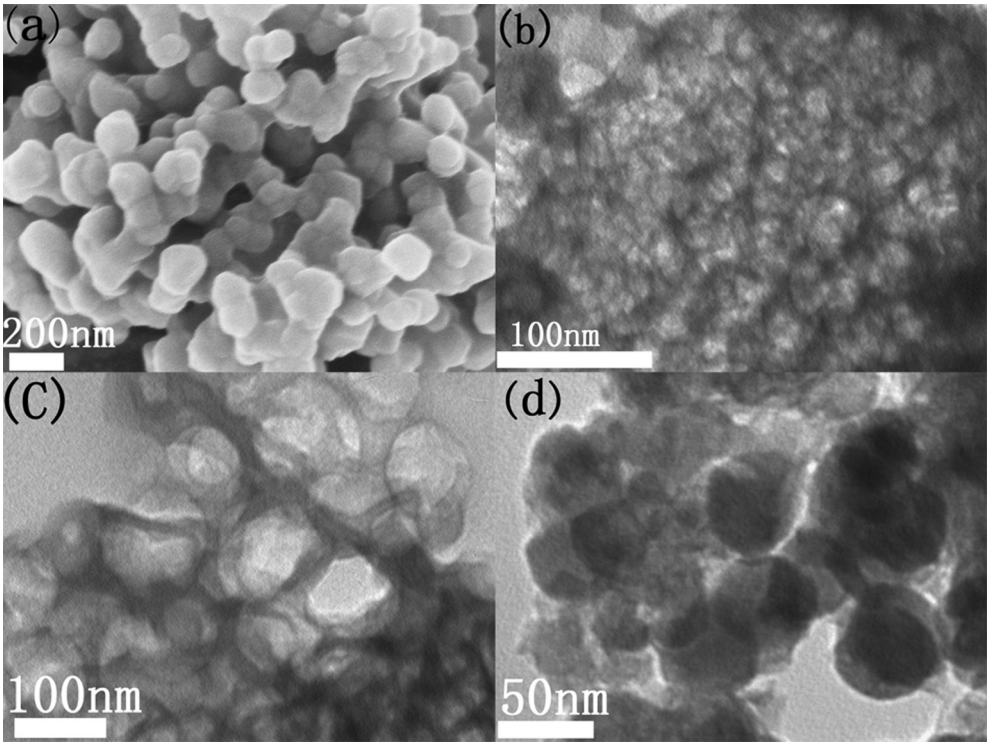

Fig. 4. (a) Scanning electron microscopy (SEM) image of Li_2MnSiO_4 products (without PEG-600), (b, c) Transmission electron images (TEM) of nest-like carbon network, (d), TEM image of sample 2 after cycling test (10 cycles).

the starting materials were mixed together and treated by ultrasonic, the PEG-600 would enwrap the nanospherical SiO_2 to form SiO_2–PEG-600 complexes. During the later heat treatment process, the PEG-600 was carbonized to form nest-like carbon network. This carbon network was helpful for suppressing the growth and agglomeration of Li_2MnSiO_4 particles. Thus Li_2MnSiO_4 particles basically keep the spherical morphology and size of corresponding SiO_2 precursor. To further learn the distribution of carbon in three-dimension, we treated the sample 1 with HCl aqueous solution to remove the Li_2MnSiO_4 nanospheres and learn the distribution of carbon. The nest-like residuals consist of carbon network can be clearly observed from the TEM image (Fig. 4b, c).

The as-prepared products were assembled into coin cells to test their electrochemical performances. As the diffusion process of Li^+ within the structure of Li_2MnSiO_4 was quite slow, so the Galvanostatic charge–discharge measurements were carried out at 0.05 C within a narrow voltage window (2.0 V–4.6 V vs. Li/Li^+) (1 C = 333 mA g^{-1}). Fig. 5a shows the charge–discharge curves of sample 2 at room temperature. The nanoparticles exhibit an initial discharge capacity of 215.3 mAh g^{-1} and a charge capacity of 340 mAh g^{-1}, the charge capacity is close to the $2Li^+$ extraction during the charge process. The discharge capacity decreases to 190.7 mAh g^{-1} and 191.2 mAh g^{-1} for the 2nd and 3rd cycles, the 2nd and 3rd cycles discharge capacities corresponded to nearly $1.1Li^+$ insertion, which is equal to 57% of the theoretical capacity. The obvious capacity loss probably results from the formation of solid electrolyte interphase (SEI) [11,29], the degradation of electrolyte under the high voltage (>4.5 V) [24], or a change in the lattice parameters caused by Jahn–Teller distortion associating with the Mn^{3+} [12,30].

Fig. 5b shows the discharge capacities and cyclic performances of sample 1 and sample 2 at 0.05 C. The initial discharge specific capacity of sample 2 is 215.3 mAh g^{-1}; after 40 cycles, sample 2 is still maintaining a high discharge capacity of 175 mAh g^{-1}. With comparison, the first discharge capacity of sample 1 is 94.1 mAh g^{-1}; after 40 cycles, sample 1 just delivers a discharge capacity of 50 mAh g^{-1}. At the same time, if the sample 2 fabricated without grapheme, it provides lower discharge capacity than sample 2 but higher than sample 1 (Fig. S3, Supporting Information). It is obvious that the sample 2 exhibits a good improvement in the electrical properties, which means the carbon network and carbon layer have a synergistic effect in terms of improving the electrochemical performance. Fig. 5c shows the cycling performance of sample 2 composite at a high current density of 0.5 C. As can be seen, the discharge capacity of sample 2 is around 114 and 90 mAh g^{-1} during the continuous cycles (40 cycles). Sample 2 exhibits a good cyclability at 0.5 C.

Fig. 5d shows the Nyquist plots of sample 1 and sample 2. Both Nyquist plots have a semicircle at middle frequency and a slope line low frequency. The semicircle is related to the charge-transfer impedance on the electrode material/electrolyte, and the slope line is related to the Li^+ diffusion in the electrode material. As shown in Fig. 5d, the semicircle part of sample 2 is smaller than that of sample 1, indicating that after coating with carbon and graphene, the electronic conductivity of sample 2 is greatly improved. Therefore, sample 2 has better electrochemical performance than sample 1.

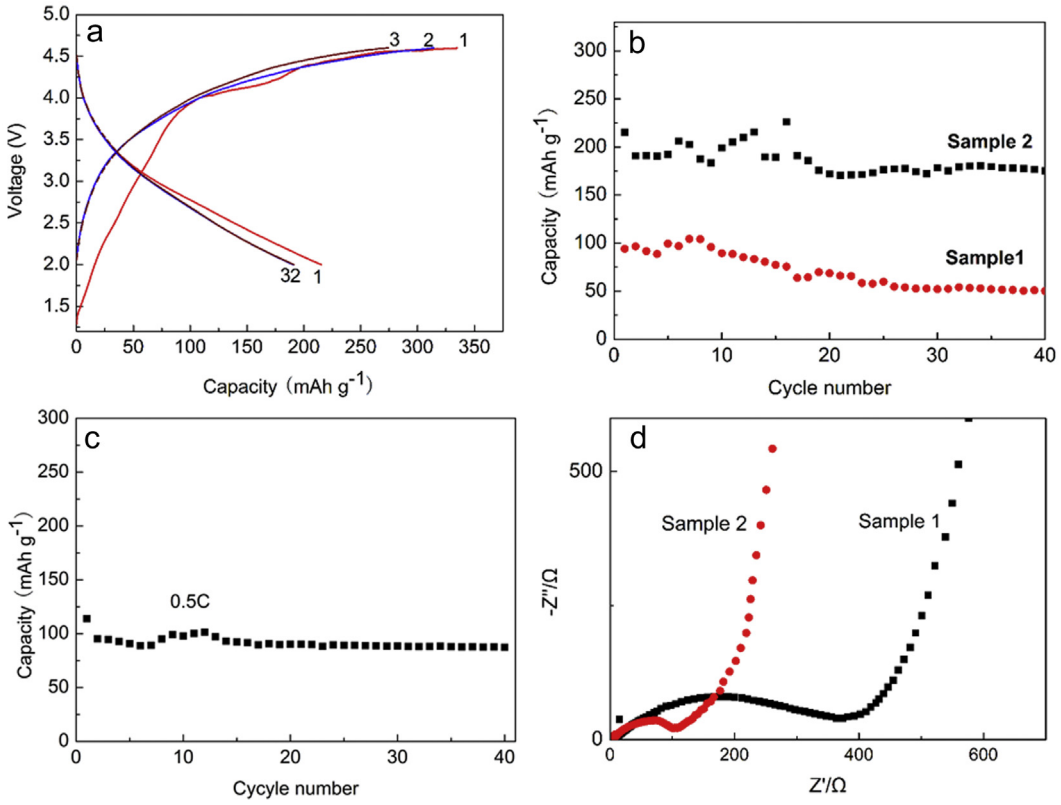

Fig. 5. (a) Charge–discharge profiles recorded at 0.05 C and room temperature of sample 2, (b) Discharge capacity vs. cycle number plots of sample 1, sample 2 at 0.05 C, (c) Discharge capacity vs. cycle number plots of sample 2 at 0.5 C, (d) Nyquist plots of sample 1 and sample 2.

The Li_2MnSiO_4/C/graphene composites show an improvement on both cycling performance and capability, which can be mainly attributed to the following reasons: Firstly, the particle size of Li_2MnSiO_4 is only 50 nm. From previous works [9,10], it can be found that nanostructure is vital for improving electrochemical performance of Li_2MnSiO_4 cathode materials. Nanospheres offer short pathways for fast moving of Li^+ and electronic from the inner to the surface of the particles. Secondly, for the Li_2MnSiO_4/C/graphene composites, uniform Li_2MnSiO_4 nanoparticles are dispersed within the nest-like carbon network (Fig. 4b, c), which can effectively prevent the agglomeration of the Li_2MnSiO_4 nanoparticles during charge/discharge. At the same time, the carbon coating (carbon and graphene sheets) with high electronic conductivity is beneficial for improving the conducting of Li_2MnSiO_4 (Fig. 5d), providing highly conductive channels for electron mobility between adjacent nanoparticles. The carbon network and carbon layer have a synergistic effect in terms of improving the electrochemical performance, which can hamper the further destruction of the crystal structure (the structure can be maintained after charge–discharge process (Fig. S1)) and effectively prevent the manganese dissolution during charge/discharge [29]. The TEM images of sample 2 after cycling test (10 cycles) is shown in Fig. 4d, which basically retains the original morphology of nanospheres. This result confirms the effect of carbon network and carbon layer during cycling. Finally, the improvement of capacity and cyclability of sample 2 is owing to the nanosize (50 nm), and the surrounding carbon/graphene matrix.

4. Conclusions

In summary, we have prepared Li_2MnSiO_4/C/graphene composites by PEG-600 assisted solid-state reaction using spherical SiO_2 as precursor, followed by heat treatment with the mixed carbon sources. The Li_2MnSiO_4 nanospheres are embedded in 3D nest-like carbon network. Electrochemical measurements showed that the composites have good electrochemical performance. The carbon network and carbon layer are favorable for improving the capability and cycling stability of Li_2MnSiO_4/C/graphene composites.

Acknowledgments

This work was supported by the National Natural Science Fund of China (no. 91022033, 21201158), the 973 Project of China (no. 2011CB935901), Anhui Provincial Natural Science Foundation (1208085QE101) and the Fundamental Research Funds for the Central Universities (no. WK 2340000027).

Appendix A. Supplementary data

Supplementary data related to this article can be found at http://dx.doi.org/10.1016/j.jpowsour.2013.07.079.

References

[1] R. Dominko, J. Power Sources 184 (2008) 462–468.
[2] G. He, G. Popov, L.F. Nazar, Chem. Mater. 25 (2013) 1024–1031.
[3] N. Jayaprakash, N. Kalaiselvi, P. Periasamy, Nanotechnology 19 (2007) 025603.
[4] D. Lv, W. Wen, X. Huang, J. Bai, J. Mi, S. Wu, Y. Yang, J. Mater. Chem. 21 (2011) 9506.
[5] M. Arroyo-de Dompablo, M. Armand, J. Tarascon, U. Amador, Electrochem. Commun. 8 (2006) 1292–1298.
[6] R. Dominko, M. Bele, A. Kokalj, M. Gaberscek, J. Jamnik, J. Power Sources 174 (2007) 457–461.
[7] S. Aono, T. Tsurudo, K. Urita, I. Moriguchi, Chem. Commun. 49 (2013) 2939.
[8] M.K. Devaraju, T. Tomai, A. Unemoto, I. Honma, RSC Adv. 3 (2013) 608.
[9] D.M. Kempaiah, D. Rangappa, I. Honma, Chem. Commun. 48 (2012) 2698.
[10] D. Rangappa, K.D. Murukanahally, T. Tomai, A. Unemoto, I. Honma, Nano Lett. 12 (2012) 1146–1151.
[11] V. Aravindan, K. Karthikeyan, S. Ravi, S. Amaresh, W.S. Kim, Y.S. Lee, J. Mater. Chem. 20 (2010) 7340.
[12] Y.-X. Li, Z.-L. Gong, Y. Yang, J. Power Sources 174 (2007) 528–532.
[13] K. Gao, C.-S. Dai, J. Lv, S.-D. Li, J. Power Sources 211 (2012) 97–102.
[14] V. Aravindan, K. Karthikeyan, S. Amaresh, Y.S. Lee, Electrochem. Solid-State Lett. 14 (2011) A33.
[15] K. Karthikeyan, V. Aravindan, S.B. Lee, I.C. Jang, H.H. Lim, G.J. Park, M. Yoshio, Y.S. Lee, J. Power Sources 195 (2010) 3761–3764.
[16] V. Aravindan, K. Karthikeyan, K.S. Kang, W.S. Yoon, W.S. Kim, Y.S. Lee, J. Mater. Chem. 21 (2011) 2470.
[17] C. Su, X. Bu, L. Xu, J. Liu, C. Zhang, Electrochim. Acta 64 (2012) 190–195.
[18] C. Sun, S. Rajasekhara, J.B. Goodenough, F. Zhou, J. Am. Chem. Soc. 133 (2011) 2132–2135.
[19] P. Lian, X. Zhu, H. Xiang, Z. Li, W. Yang, H. Wang, Electrochim. Acta 56 (2010) 834–840.
[20] Z.-S. Wu, W. Ren, L. Wen, L. Gao, J. Zhao, Z. Chen, G. Zhou, F. Li, H.-M. Cheng, ACS Nano 4 (2010) 3187–3194.
[21] S.-W. Zhang, S.-X. Zhou, Y.-M. Weng, L.-M. Wu, Langmuir 21 (2005) 2124–2128.
[22] S. Park, J. An, R.D. Piner, I. Jung, D. Yang, A. Velamakanni, S.T. Nguyen, R.S. Ruoff, Chem. Mater. 20 (2008) 6592–6594.
[23] M. Arroyo-de Dompablo, R. Dominko, J. Gallardo-Amores, L. Dupont, G. Mali, H. Ehrenberg, J. Jamnik, E. Moran, Chem. Mater. 20 (2008) 5574–5584.
[24] R. Dominko, M. Bele, M. Gaberšček, A. Meden, M. Remškar, J. Jamnik, Electrochem. Commun. 8 (2006) 217–222.
[25] I. Belharouak, A. Abouimrane, K. Amine, J. Phys. Chem. C 113 (2009) 20733–20737.
[26] V. Aravindan, K. Karthikeyan, S. Amaresh, H.S. Kim, D.R. Chang, Y.S. Lee, Ionics 17 (2010) 3–6.
[27] D. Luxembourg, G. Flamant, D. Laplaze, Carbon 43 (2005) 2302–2310.
[28] G.-Y. Zhang, Y.-Y. Xu, D.-Z. Gao, Y.-Q. Sun, J. Alloys Compd. 509 (2011) 885–890.
[29] Q. Zhang, Q. Zhuang, S. Xu, X. Qiu, Y. Cui, Y. Shi, Y. Qiang, Ionics 18 (2011) 487–494.
[30] T. Muraliganth, K.R. Stroukoff, A. Manthiram, Chem. Mater. 22 (2010) 5754–5761.